Inf-Sup-Constant-Free State Error Estimator for Model Order Reduction of Parametric Systems in Electromagnetics

Sridhar Chellappa*   Lihong Feng*   Valentín de la Rubia†   Peter Benner*

*Department of Computational Methods in Systems and Control Theory, Max Planck Institute for Dynamics of Complex Technical Systems, 39106 Magdeburg, Germany.
Email: chellappa@mpi-magdeburg.mpg.de, ORCID: 0000-0002-7288-3880
Email: feng@mpi-magdeburg.mpg.de, ORCID: 0000-0002-1885-3269
Email: benner@mpi-magdeburg.mpg.de, ORCID: 0000-0003-3362-4103
†Departamento de Matemática Aplicada a las TIC, ETSI de Telecomunicación, Universidad Politécnica de Madrid, 28040 Madrid, Spain.
Email: valentin.delarubia@upm.es, ORCID: 0000-0002-2894-6813

Abstract: A reliable model order reduction process for parametric analysis in electromagnetics is detailed. Special emphasis is placed on certifying the accuracy of the reduced-order model. For this purpose, a sharp state error estimator is proposed. Standard *a posteriori* state error estimation for model order reduction relies on the *inf-sup* constant. For parametric systems, the *inf-sup* constant is parameter-dependent. The *a posteriori* error estimation for systems with very small or vanishing *inf-sup* constant poses a challenge, since it is inversely proportional to the *inf-sup* constant, resulting in rather useless, overly pessimistic error estimators. Such systems appear in electromagnetics since the *inf-sup* constant values are close to zero at points close to resonant frequencies, where they eventually vanish. We propose a novel *a posteriori* state error estimator which avoids the calculation of the *inf-sup* constant. The proposed state error estimator is compared with the standard error estimator and a recently proposed one in the literature. It is shown that our proposed error estimator outperforms both existing estimators. Numerical experiments are performed on real-life microwave devices such as narrowband and wideband antennas, as well as a dual-mode waveguide filter. These examples show the capabilities and efficiency of the proposed methodology.

Keywords: Antennas, error analysis, finite element methods, Galerkin method, integral equation methods, microwave circuits, reduced basis methods, reduced order systems.

AMS subject classifications: 65M15, 65M60, 65R10, 78A50

Novelty statement: We propose efficient, sharp a posteriori state error estimation for reduced-order models of general linear parametric systems. Robustness of the estimator is demonstrated via its applications in computational electromagnetics. It avoids computing a quantity that normally tends to blow up existing error estimators at or near resonance frequencies. Our new estimator is integrated within an adaptive greedy algorithm that iteratively builds the reduced-order model.

1 Introduction

The rapid rise in demand for novel communication devices with an emphasis on optimal performance has posed a challenge to the standard design and prototyping workflow to manufacture such devices. As a result, a great computational effort is carried out to get physical insight from time-consuming electromagnetic simulations by means of parametric studies. The ultimate goal of these parametric analyses is to develop robust and effective electrical designs, which are of paramount importance for industry. Different efforts in the computational elec-

tromagnetic (CEM) community have been carried out to speed this costly process up and many of them follow the model order reduction (MOR) trend [1, 6–8, 21, 24, 27, 32, 36, 44].

MOR has demonstrated its robustness in reducing the complexity of parametric systems [4, 33]. Often, algorithms or methods are proposed without guaranteed accuracy, due to missing error analysis or are lacking efficiently computable error estimators. It is quite usual that the proposition of corresponding error estimation lags behind new algorithms. So far, the standard *a posteriori* state error estimator is widely used if no better choice is available, namely, residual norm divided by the *inf-sup* constant [21, 22, 33, 40]. As already stated in [17], keeping the *inf-sup* constant in the denominator of the error estimator causes risk for many problems with small *inf-sup* constants. The system of time-harmonic Maxwell's equations is one of them since it has *inf-sup* constants close to zero near to resonant frequencies. This leads to an error estimator having very large magnitude at those frequencies, even though the true error is already very small [19, 34, 37].

Some *a posteriori* error estimators independent of the *inf-sup* constant are recently proposed in [17, 39]. There, instead of computing the *inf-sup* constant, additional dual or residual systems are solved to obtain the error estimators. A state error estimator is proposed in [39], and an output error estimator is considered in [17]. The output error estimators are of interest when the accuracy of the outputs needs to be guaranteed by the reduced-order model (ROM). However, for some cases, e.g., for fast frequency sweeps in electromagnetics as well as in acoustics [19, 34], the state vector should be accurately approximated by the ROM. Therefore, state error estimation is important for generating accurate ROMs in such situations.

As the central contribution of this work, we introduce a new *a posteriori* error estimator for the state error introduced by the ROM approximation. The proposed estimator avoids computing the *inf-sup* constant. Instead, it exploits a residual system to construct the estimator. The same residual system was also used in [39]. However, our newly proposed error estimator is more accurate that the one detailed in [39], according to our analyses in Section 4.1. Further, an adaptive algorithm is proposed to iteratively build the ROM by using this new state error estimator.

The rest of the paper is organized as follows. In Section 2, we introduce the parametric problem in electromagnetics considered in this work, and the standard state error estimation. The new state error estimation is proposed in Section 3. The estimator proposed in [39] is reviewed and theoretically compared with our proposed estimator in Section 4. Numerical simulations in Section 5 show the performance of the proposed estimator, as well as the results of the standard estimator and the estimator

in [39]. Finally, in Section 6, we provide conclusions.

2 Parametric Problem and Standard State Error Estimation

The systems we are interested in are steady (time-harmonic), linear, parametric systems in the form of,

$$A(\mu)x(\mu) = B(\mu). \tag{1}$$

Here, $\mu \in \mathbb{C}^m$ is the vector of parameters, $A(\mu) \in \mathbb{C}^{n \times n}$, $B(\mu) \in \mathbb{C}^{n \times p}$ are system matrices, and $x(\mu) \in \mathbb{C}^{n \times p}$ is the state solution, n is assumed to be large, say $n \in \mathcal{O}(10^5)$. System (1) is referred to as the full order model (FOM). Such systems arise from numerical discretization of partial differential equations (PDEs) and integral equations (IEs), such as the time-harmonic Maxwell's equations where differential and integral approaches are both possible.

The ROM can be obtained based on Galerkin projection,

$$\hat{A}(\mu)z(\mu) = \hat{B}(\mu), \tag{2}$$

where the reduced matrices are given by $\hat{A}(\mu) = V^T A(\mu)V \in \mathbb{C}^{r \times r}$, $\hat{B}(\mu) = V^T B(\mu) \in \mathbb{C}^{r \times p}$ and $V \in \mathbb{R}^{n \times r}$ is the projection matrix spanning the reduced space. $z(\mu) \in \mathbb{C}^{r \times p}$ stands for the reduced state vector. $r \ll n$ is the order of the ROM. The approximate state vector obtained from the ROM is $\hat{x}(\mu) = Vz(\mu)$, such that $x(\mu) \approx \hat{x}(\mu)$. By considering each column of $B(\mu)$ separately, the error estimators presented in the following can be easily extended for systems with multiple inputs [17]. Please also refer to the details in Section 5, where a circuit with two ports is used to test the error estimators. For simplicity of explanation in the following sections, we assume that $B(\mu)$ is a vector.

Next, we introduce the standard state error estimation and point out the role of the *inf-sup* constant.

2.1 Standard State Error Estimation

The residual obtained by substituting the approximate solution into the FOM is given by

$$r(\mu) = B(\mu) - A(\mu)\hat{x}(\mu). \tag{3}$$

Then from (1), we obtain,

$$r(\mu) = A(\mu)x(\mu) - A(\mu)\hat{x}(\mu), \tag{4}$$

so that

$$\|x(\mu) - \hat{x}(\mu)\| = \|A(\mu)^{-1}r(\mu)\|. \tag{5}$$

The standard *a posteriori* state error estimation is obtained by invoking the sub-multiplicativity property of the operator norm in (5). Considering the 2-norm, it can

be shown that the error $e(\mu) := x(\mu) - \hat{x}(\mu)$ is bounded above and below by the residual $r(\mu)$ as

$$\frac{1}{\sigma_{\max}}\|r(\mu)\| \leq \|e(\mu)\| \leq \frac{1}{\sigma_{\min}}\|r(\mu)\| \qquad (6)$$

with $\sigma_{\max}$ and $\sigma_{\min}$ the largest and smallest singular values of $A(\mu)$, respectively. Through this inequality, we define the upper bound for the state approximation error

$$\|e(\mu)\| = \|x(\mu) - \hat{x}(\mu)\| \leq \frac{1}{\sigma_{\min}}\|r(\mu)\| =: \delta(\mu). \qquad (7)$$

Further, in this discretized setting, $\sigma_{\min}$ plays the role of the *inf-sup* constant. However, the standard error estimator $\delta(\mu)$ approaches infinity when the matrix $A(\mu)$ is close to singular at some values of μ, resulting in a rather poor estimation and a naive bound. This is true for many problems [17]. Furthermore, the above error estimation leads to unacceptable overestimation of the state error even for well-conditioned problems [38]. Given no better choices, the residual norm $\|r(\mu)\|$ is often used as a heuristic error estimator [2,10–12,18,30,35,41,42]. In Section 5, we also numerically compare the proposed error estimator with the residual norm $\|r(\mu)\|$.

3 Proposed State Error Estimation

From (4), we know that

$$A(\mu)(x(\mu) - \hat{x}(\mu)) = r(\mu).$$

To compute the error $e(\mu)$ for each value of μ, we need to solve the residual system corresponding to each μ:

$$A(\mu)e(\mu) = r(\mu). \qquad (8)$$

Note that the residual system (8) is of the original large dimension n. It is not practical to solve many large systems at many values of μ in order to know the error distribution in the whole parameter domain. For fast error estimation, we first construct the ROM of the residual system using a projection matrix $V_{\mathrm{e}} \in \mathbb{R}^{n \times \ell}$ that spans the error subspace. This is given as,

$$\tilde{A}(\mu)z_e(\mu) = \tilde{r}_{\mathrm{pr}}(\mu), \qquad (9)$$

where $\tilde{A}(\mu) = V_{\mathrm{e}}^T A(\mu) V_{\mathrm{e}}$, $\tilde{r}_{\mathrm{pr}}(\mu) = V_{\mathrm{e}}^T r(\mu)$, and $\tilde{e}(\mu) := V_{\mathrm{e}} z_e(\mu)$ approximates $e(\mu)$. Then, our proposed state error estimation is given by $\|\tilde{e}(\mu)\|$, i.e.

$$\|x(\mu) - \hat{x}(\mu)\| = \|e(\mu)\| \approx \|\tilde{e}(\mu)\|. \qquad (10)$$

We obtain the following analysis for the rigorousness and tightness of the state error estimator $\|\tilde{e}(\mu)\|$.

Theorem 1. *The state error $\|e(\mu)\|$ can be bounded by $\|\tilde{e}(\mu)\|$ as follows:*

$$\|\tilde{e}(\mu)\| - \gamma(\mu) \leq \|e(\mu)\| \leq \|\tilde{e}(\mu)\| + \gamma(\mu). \qquad (11)$$

Here $\gamma(\mu) = \|e(\mu) - \tilde{e}(\mu)\| \geq 0$ is a small value if $\tilde{e}(\mu)$ well approximates $e(\mu)$, which is achievable by accurate MOR of the residual system (8).

The theorem can be easily proved by applying the triangular inequality to $\|e(\mu) - \tilde{e}(\mu)\|$, and is not detailed here.

Remark 1. *Theorem 1 is also valid for a complex matrix $V \in \mathbb{C}^{n \times r}$. Considering that a real matrix V is used in our numerical tests (see Remark 5), we keep V real all through the paper to avoid confusion.*

3.1 Computing the State Error Estimator

In order to compute the state error estimator $\|\tilde{e}(\mu)\|$, we need to construct the ROM (9) for the residual system (8). Consequently, the projection matrix V_{e} has to be computed. In a similar manner as in [17], we look at the residual system (8) in order to identify the subspace for the trajectory of the state error vector $e(\mu)$:

$$\begin{aligned} e(\mu) &= A(\mu)^{-1}r(\mu) \\ &= A(\mu)^{-1}(B(\mu) - A(\mu)\hat{x}(\mu)) \\ &= A(\mu)^{-1}B(\mu) - \hat{x}(\mu) \\ &= A(\mu)^{-1}B(\mu) - Vz(\mu). \end{aligned} \qquad (12)$$

Note that $A(\mu)^{-1}B(\mu)$ is nothing but the state solution $x(\mu)$. If we could find a subspace to approximate the trajectory of $x(\mu)$, say range(V_r), then $x(\mu)$ can be approximately represented by the columns of V_r, i.e. $x(\mu) \approx V_r z_r(\mu)$. Thus,

$$\begin{aligned} e(\mu) &= A(\mu)^{-1}B(\mu) - Vz(\mu) \\ &\approx V_r z_r(\mu) - Vz(\mu). \end{aligned} \qquad (13)$$

Since the state error vector $e(\mu) \neq 0$, range(V_r) should be different from range(V) used for constructing the original system ROM (2). It is clear from (13) that $e(\mu)$ can be approximated by linear combination of the columns in V_r and V. Therefore, we can construct V_e as

$$V_e = \mathrm{colspan}\{V_r, V\}. \qquad (14)$$

In the next subsection, we propose an algorithm for constructing the ROM (2) of the original FOM (1) by using the proposed state error estimator $\|\tilde{e}(\mu)\|$.

3.2 Constructing the ROM

The algorithm for constructing the ROM (2) is detailed in Algorithm 1, where the proposed state error estimator is used to select samples of the parameter μ for computing the projection matrix V. We make some remarks to highlight various aspects of Algorithm 1.

- The algorithm is automatic. The user needs only to provide a training set Ξ. Adaptive sampling approaches for iteratively updating the training set

exist [5, 16, 23, 26] and can be combined with Algorithm 1. Since it is not the focus of the paper, we will present the corresponding algorithm elsewhere.

- In Steps 3-4, parameter dependent matrices $V(\mu^*)$ and $V_r(\mu_e^*)$ can be computed using a favorite MOR method. When using the reduced basis method, we have

$$V(\mu^*) = A(\mu^*)^{-1}B(\mu^*), \ V_r(\mu_e^*) = A(\mu_e^*)^{-1}B(\mu_e^*).$$

  In [17], a multi-moment-matching method [3] is used to compute $V(\mu^*)$, which can also be used to compute $V_r(\mu_e^*)$. We do not repeat the details in this work.

- It is important that the parameter samples μ^* and μ_e^* must be different, otherwise, this may lead to $V = V_r$, which is in contradiction with the analysis in Subsection 3.1 (see (13)). Therefore, we choose two different initial samples, and select two different sequential ones in Step 7 and Step 8, respectively. In Step 8, we simply use $\|r_e(\mu)\|$, the residual norm introduced by $\tilde{e}(\mu)$, the approximate solution to the residual system (8), as the indicator for selecting μ_e^* in a greedy strategy.

- ϵ is taken as the maximal value of the state error estimator, i.e. $\|\tilde{e}(\mu^*)\|$.

4 Review of the Randomized State Error Estimator

A randomized state error estimator is proposed in [39] for Galerkin projection based MOR. It is stated that the $\|\cdot\|_\Sigma$ norm of the state error satisfies

$$\|e\|_\Sigma^2 = e^T\Sigma e = e^T\mathbb{E}(zz^T)e = \mathbb{E}((z^Te)^2), \quad (15)$$

where $z \in \mathbb{R}^n$ is a zero mean Gaussian random vector with covariance matrix $\Sigma \in \mathbb{R}^{n \times n}$.

An approximation to $\mathbb{E}((z^Te)^2)$ is firstly proposed,

$$\mathbb{E}((z^Te)^2) \approx \big(\frac{1}{K}\sum_{i=1}^{K}(z_i^Te)^2\big)^{1/2}, \quad (16)$$

where $z_i \in \mathbb{R}^n$ are K samples of z. After simple derivations, it is proved that [39]

$$\big(\frac{1}{K}\sum_{i=1}^{K}(z_i^Te)^2\big)^{1/2} = \big(\frac{1}{K}\sum_{i=1}^{K}(\xi_i(\mu)^Tr(\mu))^2\big)^{1/2}, \quad (17)$$

where $r(\mu)$ is the residual defined in (3) and the parametric functions $\xi_i(\mu), i = 1, \ldots, K$, satisfy the following K random dual systems, respectively,

$$A(\mu)^T\xi_i(\mu) = z_i, \quad 1 \le i \le K. \quad (18)$$

Algorithm 1 Constructing the ROM (2) using the state error estimator $\|\tilde{e}(\mu)\|$

Input: System matrices $A(\mu), B(\mu)$, training set Ξ including a certain number of samples of μ, tolerance `tol` for the acceptable state error.
Output: ROM (2).
1: Initialize $V = [\,], V_e = [\,], \epsilon = 1 + \texttt{tol}$. Two different samples μ^* and μ_e^* randomly taken from Ξ.
2: **while** $\epsilon > \texttt{tol}$ **do**
3: Compute $V(\mu^*)$ using a favorite MOR method and update V: $V = \mathsf{orth}([V, V(\mu^*)])$.
4: Compute $V_r(\mu_e^*)$ using a favorite MOR method and update V_r: $V_r = \mathsf{orth}([V_r, V_r(\mu_e^*)])$.
5: If a real V is preferable, then $V := \mathsf{orth}[\mathrm{real}(V), \mathrm{imag}(V)]$; also, if a real V_r is preferred, then $V_r := \mathsf{orth}[\mathrm{real}(V_r), \mathrm{imag}(V_r)]$.
6: Form V_e: $\mathrm{range}(V_e) = \mathrm{colspan}\{V_r, V\}$.
7: Compute the estimated state error vector $\tilde{e}(\mu)$ using V and V_e.
8: Choose the next sample μ^* from Ξ as

$$\mu^* = \arg\max_{\mu \in \Xi}\|\tilde{e}(\mu)\|.$$

9: Choose the next sample μ_e^* from Ξ following

$$\mu_e^* = \arg\max_{\mu \in \Xi}\|r_e(\mu)\|.$$

  Here $r_e(\mu) = r(\mu) - A(\mu)\tilde{e}(\mu)$ is the residual introduced by $\tilde{e}(\mu)$.
10: $\epsilon = \|\tilde{e}(\mu^*)\|$.
11: **end while**
12: Use V to construct the ROM: $\hat{A}(\mu) = V^TA(\mu)V$, $\hat{B}(\mu) = V^TB(\mu)$.

To define the error estimator, reduced systems for those K random dual systems are first constructed as,

$$V_{rd}^TA(\mu)^TV_{rd}\hat{\xi}_i(\mu) = V_{rd}^Tz_i, \quad 1 \le i \le K.$$

Then $\xi_i(\mu)$ can be approximated by $V_{rd}\hat{\xi}_i(\mu)$ as $\xi_i(\mu) \approx \tilde{\xi}_i(\mu) := V_{rd}\hat{\xi}_i(\mu)$. Finally, the state error estimator is defined as

$$\tilde{\Delta}(\mu) = \big(\frac{1}{K}\sum_{i=1}^{K}(\tilde{\xi}_i(\mu)^Tr(\mu))^2\big)^{1/2}. \quad (19)$$

It is proved in [39] that if $V_{rd} = V_e$, then $\tilde{\Delta}(\mu)$ in (19) can be written as

$$\tilde{\Delta}(\mu) = \big(\frac{1}{K}\sum_{i=1}^{K}(z_i^T\tilde{e}(\mu))^2\big)^{1/2}. \quad (20)$$

Note that V_e and $\tilde{e}(\mu)$ are defined in (9). This means, with the assumption $V_{rd} = V_e$, $\tilde{\Delta}(\mu)$ is an average of K inner products of z_i and $\tilde{e}(\mu)$, $i = 1, \ldots, K$.

4.1 Comparison between $\tilde{\Delta}(\mu)$ and $\|\tilde{e}(\mu)\|$

- It is clear that $\tilde{\Delta}(\mu)$ is an approximation to $\left(\frac{1}{K}\sum_{i=1}^{K}(\xi_i(\mu)^T r(\mu))^2\right)^{1/2}$ in (17). The approximation is caused by MOR for the K random dual systems in (18); or alternatively by MOR for the residual system (8) if $\tilde{\Delta}(\mu)$ in (20) is considered. Combining (15), (16) and (17), we see that $\left(\frac{1}{K}\sum_{i=1}^{K}(\xi_i(\mu)^T r(\mu))^2\right)^{1/2}$ is again an approximation to the state error $\|e\|_\Sigma$. Whereas, our proposed state error estimator $\|\tilde{e}\|$ is a direct approximation to the state error $\|e\|$, where the approximation is only introduced by MOR for the residual system (8). If similar accuracy of MOR for both error estimators is obtained, then $\|\tilde{e}\|$ should be more accurate than $\tilde{\Delta}(\mu)$.

- For computing $\tilde{\Delta}(\mu)$, no efficient method is proposed in [39] to compute the projection matrix V_e for the reduced residual system (9). Instead, two algorithms are proposed [39, Algorithms 3.1, 3.2] to compute V_{rd} and reduce the K random dual systems (18). In contrast, we have proposed an efficient method of computing V_e in subsection 3.1, so that only one system needs to be reduced.

- If $\|\cdot\|_2$ is used for both error estimators, then Σ for $\|e\|_\Sigma$ is the identity matrix, according to (15).

5 Numerical Results

We test the proposed state error estimator $\|\tilde{e}(\mu)\|$ and the existing ones on four different real-life applications. The first is a dual-mode circular waveguide filter, and two excitation ports are considered. The other three examples include models of narrowband and wideband antennas, where only one excitation port is taken into account. After numerical discretization of the time-harmonic Maxwell's equations by means of the finite element method (FEM), the systems can be written in the form of (1). The in-house code for FEM simulations uses a second-order first family of Nédélec's elements [25,31] on meshes provided by Gmsh [20]. Fast frequency sweep is considered in all the examples. As a result, only one parameter models are taken into account in this work with $\mu = s := \jmath 2\pi f$. Here, s is the complex frequency variable, $\jmath$ is the imaginary unit, and f is the frequency with unit Hz. The system matrix has the affine form given by,

$$A(s) := \mathcal{S} + s\mathcal{U} + s^2\mathcal{T},$$

where $\mathcal{S}$ is the stiffness matrix, $\mathcal{T}$ is the mass matrix and $\mathcal{U}$ is the FEM matrix related to the first-order absorbing boundary conditions (ABC) and $\mathcal{S},\mathcal{U},\mathcal{T} \in \mathbb{R}^{n\times n}$. $B(s) := s\mathcal{Q}$ with $\mathcal{Q} \in \mathbb{R}^{n\times p}$, with p being the number of ports

and $\mathcal{Q}$ being a matrix related to the excitation currents at the ports. Finally, the state solution $x(s) \in \mathbb{C}^{n\times p}$ stands for the electric field in the analysis domain. It should be pointed out that integral equation methods for electromagnetic scattering can be taken into account as parametric problems in (1) [30,43]. By the same token, other parameters than frequency are also possible [9].

In our experiments, we define the true error (ϵ_{true}) based on the number of input ports. We first consider the error for each column $x_i(s)$ of the solution $x(s)$ separately and define the *maximal* true error as,

$$\epsilon_{\text{true}} = \max_{\substack{i\in\{1,\ldots,p\}\\ s\in\Xi}} \|x_i(s) - \hat{x}_i(s)\|,$$

where $\hat{x}_i(s)$ is the i-th column of the approximate solution $\hat{x}(s)$. Here, Ξ denotes the training set consisting of elements sampled from the parameter space. Note that for each i, the system of $x_i(s)$ is a single input system, i.e. $A(s)x_i(s) = B_i(s)$, where $B_i(s)$ is the i-th column of $B(s)$. We use the *maximal error estimator* to estimate ϵ_{true}:

$$\epsilon_{\text{est}} = \max_{\substack{i\in\{1,\ldots,p\}\\ s\in\Xi}} \Delta_i(s).$$

$\Delta_i(s)$ refers to any of the four error estimators used to estimate the error $\|x_i(s) - \hat{x}_i(s)\|$: the residual norm $\|r(s)\|$ (3), the standard error estimator $\delta(s)$ (7), the randomized error estimator $\tilde{\Delta}(s)$ (20), and the proposed state error estimator $\|\tilde{e}(s)\|$ (10). We use the metric of effectivity to gauge how close the estimated error is to the true error: $\texttt{eff} := \frac{\text{Error estimator}}{\text{True error}} = \frac{\epsilon_{\text{est}}}{\epsilon_{\text{true}}}$. For each of the four examples considered, we evaluate the performance of the four error estimators. In the sequel,

- Test 1 refers to the greedy algorithm with the standard error estimator $\delta(s)$,

- Test 2 denotes the greedy algorithm employing the residual norm $\|r(s)\|$ as a heuristic error estimator,

- Test 3 uses the randomized error estimator $\tilde{\Delta}(s)$ from [39], to drive the greedy algorithm and

- Test 4 consists of the proposed error estimator $\|\tilde{e}(s)\|$ in the greedy algorithm.

In all numerical tests, the vector 2-norm $\|\cdot\|_2$ is used for both the true and estimated errors.

Remark 2. *Note that the error ϵ_{true} and error estimators are defined for the* scaled *solution after scaling the right hand side matrix $B(s)$ with a proper scaling constant in order to avoid large norm of the solution $x(s)$. This is due to the fact that the entries in the left hand side matrix $A(s)$ have much smaller magnitudes than those in $B(s)$ because of the large value of s associated with $\mathcal{Q}$. Without scaling, both $x(s)$ and $\hat{x}(s)$ have large norms,*

leading to large absolute errors, which cannot reflect the real accuracy of the ROM. Therefore, we first scale the right hand side and then construct the ROM. The approximate solution $\hat{x}(s)$ can be recovered by scaling back without losing any accuracy. The scaling constant we take here is $scale = 10^5$, and the right hand side after scaling is $s\mathcal{Q}/scale$.

Remark 3. *Algorithm 1 is tailored for the proposed error estimator $\|\tilde{e}\|$, which can be seen from Steps 7-8 of the algorithm. Similar greedy algorithms can be developed for the other three error estimators. To avoid redundancy, we do not list the corresponding algorithms for those estimators. However, we should point out that although we use the same name: greedy algorithm for all the error estimators, they are not the same algorithm, but the corresponding algorithm for each of the estimators. The fact that greedy algorithms may be different with different error estimators is mainly due to the fact that different computational steps (e.g., projection matrices) could be involved in computing the error estimators. For example, instead of V_e, V_{rd} is needed for computing the randomized error estimator $\tilde{\Delta}(s)$. In particular, we use the greedy algorithm proposed in [39] for the randomized estimator.*

Remark 4. *For the randomized error estimator $\tilde{\Delta}(s)$ in Test 3, we make use of Algorithm 3.1 from [39] to construct V_{rd}, where a separate greedy algorithm is used. For this purpose, tol_{rd} is defined to be the tolerance for this separate greedy procedure to generate V_{rd}.*

Remark 5. *For the three antenna examples in this work, the state vectors are complex, so that the projection matrix V obtained in Steps 3-4 of Algorithm 1 is complex. However, the system matrices $\mathcal{S}, \mathcal{U}, \mathcal{T}$ are all real. To make the reduced matrices $\hat{\mathcal{S}}, \hat{\mathcal{U}}, \hat{\mathcal{T}}$ also real, we use $V := orth([real(V), imag(V)])$ (in MATLAB® notation) to construct a real projection matrix. In fact, the columns of this new real V span a subspace over $\mathbb{R}$ which is isomorphic to the one spanned by the original complex V over $\mathbb{C}$.*

For the first example, the simulations were performed on a laptop with Intel® Core™ i5-7200U @ 2.5 GHz, with 8 GB of RAM in MATLAB® 2015a. Owing to the large size of the models, the simulations for the three antenna examples were performed on a workstation with 3 GHz Intel® Xeon E5-2687W v4 processor and 256 GB of RAM, with MATLAB® 2017a. It should be pointed out that, in our experiments, the CPU time performance is not optimized, since MATLAB® code is used in the numerical computations. However, a fair comparison among the different methodologies is taken into account.

5.1 Example I : Dual-Mode Circular Waveguide Filter

Fig. 1 shows a dual-mode circular waveguide filter as well as its geometry dimensions and mesh for FEM analysis.

The scattering parameter response of this filter is detailed in Fig. 2. Dual-mode filters are widely used in satellite communication, due to their power handling capabilities [10,14]. We consider a system with $p = 2$ input ports. The dimension of the system is $n = 36,426$ and the system matrix is $A(s) = \mathcal{S} + s^2\mathcal{T}$. This time, we solve for the E-wall cavity problem and no ABC is needed, as a result, $\mathcal{U} \equiv 0$. The frequency band of interest is [11.5, 12] GHz. The tolerance for the state error of the ROM is set to be $tol = 10^{-6}$. The training set Ξ for Algorithm 1 is made up of 101 uniformly sampled $f \in [11.5, 12]$ GHz.

5.1.1 Test 1. Standard error estimator

For the first test, we use the standard error estimator $\delta(s)$, which involves computing the *inf-sup* constant. Calculating the *inf-sup* constant for all parameters in the training set is expensive. Fig. 3a shows that the greedy algorithm requires 11 iterations to converge to the defined tolerance. Fig. 3b plots the effectivity changing with iteration number. It is of order $\mathcal{O}(100)$, showing that $\delta(s)$ is not sharp. The algorithm results in a ROM of size 20.

5.1.2 Test 2. Residual norm as a heuristic error estimator

We use the norm of the residual $\|r(s)\|_2$ as an estimator for the state error. Fig. 4a illustrates the convergence of the corresponding greedy algorithm which stops within 10 iterations. The effectivity in Fig. 4b is of order $\mathcal{O}(10)$. The algorithm results in a ROM of size 20.

5.1.3 Test 3. Randomized error estimator

To compute the randomized estimator $\tilde{\Delta}(\mu)$ from [39], $K = 20$ random vectors are generated from a normal distribution by the MATLAB® command mvnrnd with seed 0, using the MersenneTwister random number generator. The projection matrix V_{rd} is constructed for the K random dual systems in (18), using Algorithm 3.1 in [39] with $tol_{rd} = 0.5$. It is seen from Fig. 5a that the greedy algorithm takes 8 iterations to converge leading to a ROM of order 16. In Fig. 5b, the effectivity of $\tilde{\Delta}(\mu)$ is plotted. Although it is close to one, there are obvious underestimations at some iterations. Furthermore, generating V_{rd} takes considerable time as shown in Table 1, even for relatively large error tolerances ($\sim \mathcal{O}(10^{-1})$).

5.1.4 Test 4. Proposed error estimator

The performance of $\|\tilde{e}(s)\|_2$ is tested by using Algorithm 1. As illustrated in Fig. 6, Algorithm 1 needs 8 iterations to converge with effectivity very close to 1. Compared with the standard error estimator $\delta(\mu)$ and the
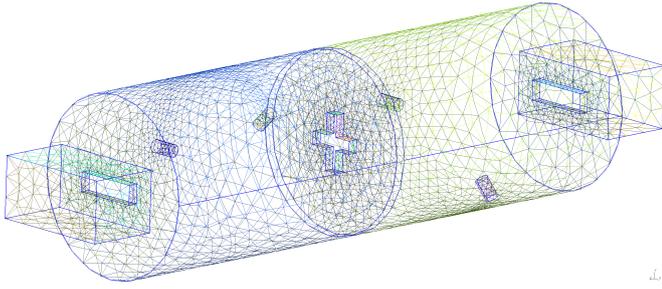
Figure 1: Dual-mode circular waveguide filter. Cavity length 43.87 mm, radius 14 mm, iris thicknesses 1.5 mm, slot lengths 10.05 mm, slot widths 3 mm, arm widths 2 mm, horizontal arm length 7.65 mm, vertical arm length 8.75 mm, tunning screw depth 3.59 mm and coupling screw depth 3.31 mm.
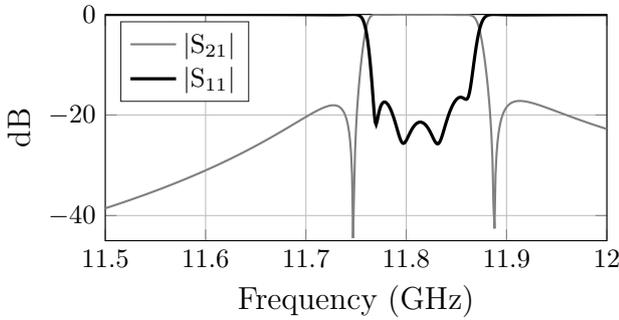

Figure 2: Dual-mode circular waveguide filter scattering parameter response.

residual norm error estimator $\|r(\mu)\|_2$, $\|\tilde{e}(s)\|_2$ is much tighter, and therefore converges faster leading to a ROM of smaller order $r = 16$. It is also more reliable than the randomized estimator $\tilde{\Delta}(\mu)$ with almost no underestimation. For the next set of tests, we consider three different antenna models:

(i) Substrate Integrated Waveguide (SIW) antenna.

(ii) Antipodal Vivaldi (AV) antenna.

(iii) Dielectric Resonator (DR) antenna.

For each of the models, we perform Tests 2, 3 and 4, as for Example I. For these examples, performing Test 1 is computationally expensive; moreover, the resulting estimation of the error is not sharp, just like in Example I. Therefore, for the remaining examples, we do not show the additional results involving the standard error estimator.
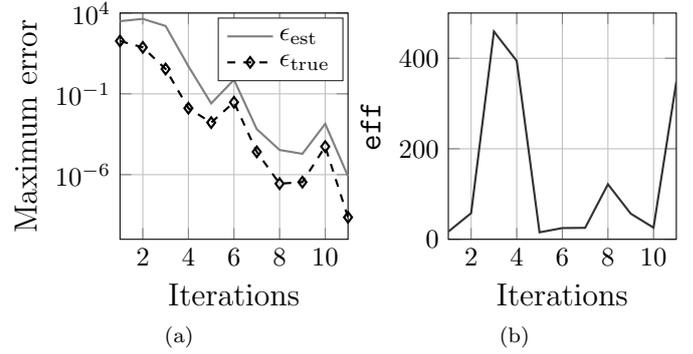
Figure 3: Dual-mode circular waveguide filter: results for Test 1. (a) Convergence of the greedy algorithm. (b) Effectivity (`eff`).
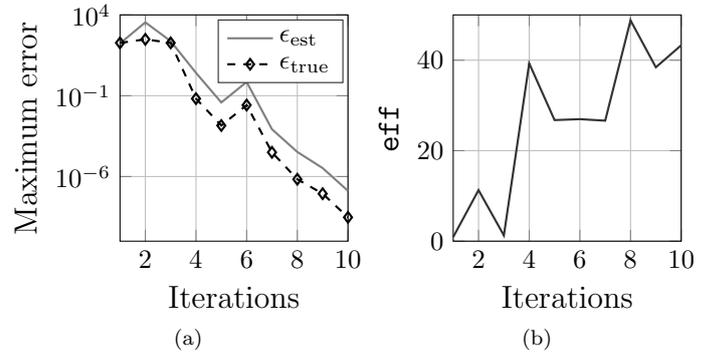
Figure 4: Dual-mode circular waveguide filter: results for Test 2. (a) Convergence of the greedy algorithm. (b) Effectivity (`eff`).
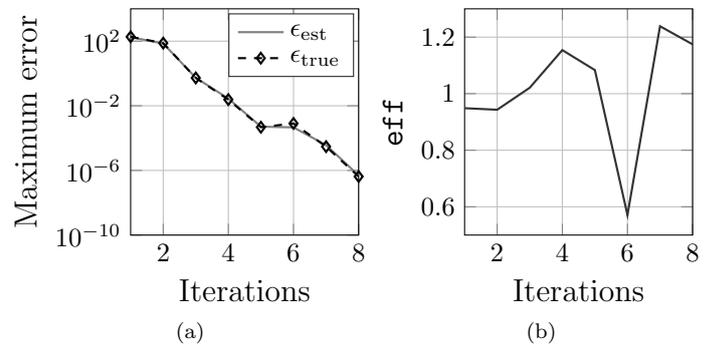
Figure 5: Dual-mode circular waveguide filter: results for Test 3. (a) Convergence of the greedy algorithm. (b) Effectivity (`eff`).
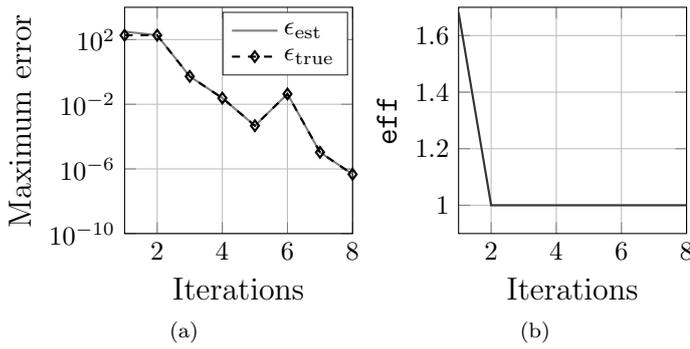
(a)   (b)

Figure 6: Dual-mode circular waveguide filter: results for Test 4. (a) Convergence of Algorithm 1. (b) Effectivity (`eff`).

5.2 Example II : Substrate Integrated Waveguide Antenna

Such antennas have gained popularity recently owing to their low-cost and efficiency [15]. Fig. 7 shows the model of the antenna along with the mesh used for its discretization. The input reflection coefficient response at the coaxial port is depicted in Fig. 8. The system is of order $n = 390,302$, with just one input. The frequency band of interest is [6, 9] GHz. The training set Ξ consists of 61 uniformly sampled parameters from this band. The tolerance (`tol`) for the greedy algorithm is set as 10^{-4}.

5.2.1 Test 2. Residual norm as a heuristic error estimator

We illustrate the convergence of the greedy algorithm using the residual estimator in Fig. 9a. The algorithm converges in 8 iterations to a ROM of size $r = 16$. The effectivity shown in Fig. 9b is less than one for the first four iterations, meaning the estimator underestimates the true error. For the next four iterations, it is of order $\mathcal{O}(10)$. Using the residual norm as an error estimator enjoys the advantage that it is very easy to implement, with only marginal overhead costs in terms of computation. However, in general, it is a crude approximation to the actual error.

5.2.2 Test 3. Randomized error estimator

Next, we use the error estimator from [39]. We use $K = 5$ randomly distributed vectors, each of length n to construct V_{rd}. The random number generator `MersenneTwister` was used with the seed set to 1. The tolerance used to obtain V_{rd} is $\texttt{tol}_{rd} = 1$. Even for such a crude tolerance, the algorithm requires around 80 minutes to converge. The long time to converge and the lack of any *a priori* knowledge to choose the number of random vectors K and the
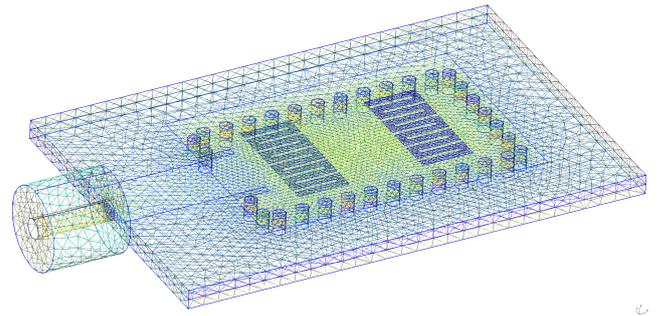

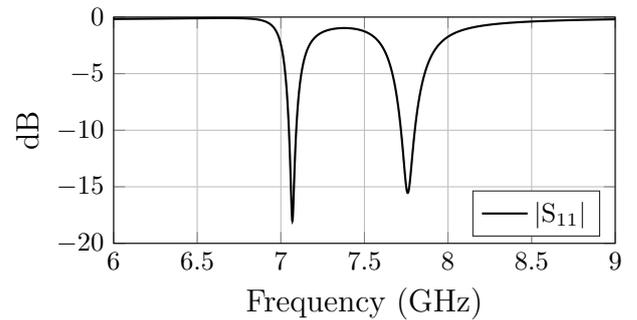Figure 7: Geometry of the SIW antenna proposed in [15].

Figure 8: Reflection coefficient at the coaxial port for the SIW antenna.

tolerance are the main disadvantages of using this algorithm. Fig. 10 shows the convergence of the greedy algorithm and the effectivity. The overall procedure requires 7 iterations to converge to a ROM of dimension $r = 14$.

5.2.3 Test 4. Proposed error estimator

For the proposed error estimator, we show the results of Algorithm 1 in Fig. 11. It requires 7 iterations to converge to a ROM with $r = 14$. The overall time to converge was around 50 minutes, much less than the time required to precompute V_{rd} in Test 3. Further, compared to the other methods, the proposed method achieves a better effectivity, where only at the first two iterations, the error estimator underestimates the true error. This is quite reasonable, since at those stages the ROM of the residual system (8) is not yet accurate enough, leading to large $\gamma(\mu)$ in (11).

5.3 Example III : Antipodal Vivaldi Antenna

For the next example, we employ an Antipodal Vivaldi antenna. It is known for good wide-band impedance performance [29]. The discretized model, shown in Fig. 12 is of dimension $n = 283,846$ with $f \in [1, 6]$ GHz being the parameter space of interest. The input reflection coefficient at the coaxial port of the optimized Antipodal
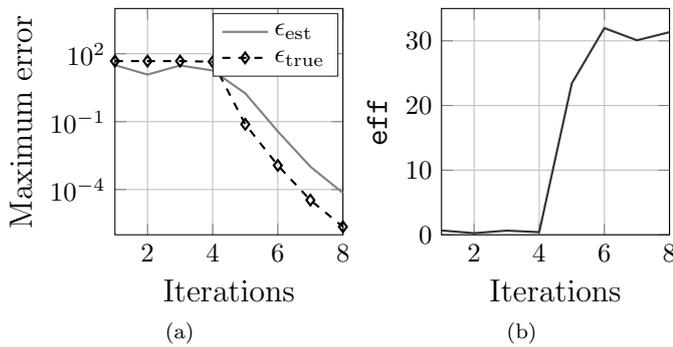
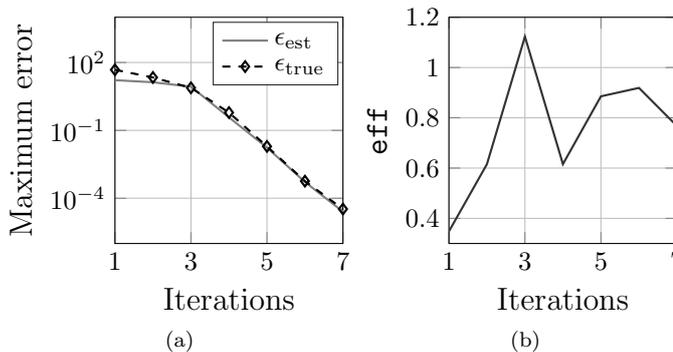Figure 9: SIW antenna: results for Test 2. (a) Convergence of the greedy algorithm. (b) Effectivity (`eff`).

Figure 10: SIW antenna: results for Test 3. (a) Convergence of the greedy algorithm. (b) Effectivity (`eff`).
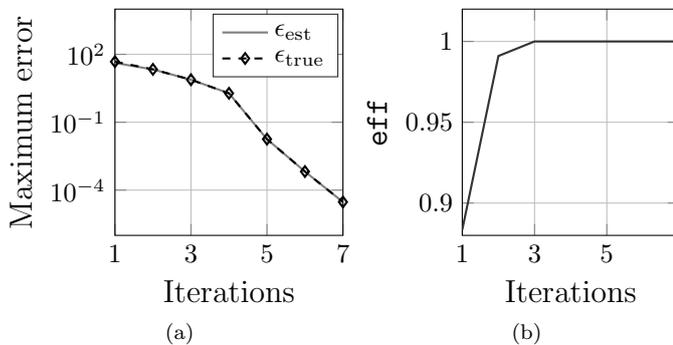

Figure 11: SIW antenna: results for Test 4. (a) Convergence of Algorithm 1. (b) Effectivity (`eff`).

Vivaldi antenna is detailed in Fig. 13. This model is particularly challenging to approximate with MOR techniques, owing to the larger number of in-band resonances. The tolerance for the ROM is set as 10^{-3}. The training set is made up of 51 uniform samples from the parameter range of interest.

5.3.1 Test 2. Residual norm as a heuristic error estimator

As noted previously, the Antipodal Vivaldi antenna is a challenging model to approximate with MOR techniques. This is evident from Fig. 14a, where the convergence of the greedy algorithm is shown. The algorithm requires up to 20 iterations to achieve the set tolerance. For this model, the norm of the residual overestimates the true error by roughly one order of magnitude, as seen in Fig. 14b, where the effectivity is illustrated. The resulting ROM has dimension $r = 40$.

5.3.2 Test 3. Randomized error estimator

To construct V_{rd} for this example, we draw $K = 6$ random vectors using the `mvnrnd` command and set tol_{rd} to be 1. The random number generator `MersenneTwister` was used with the seed set to 1. The procedure based on Algorithm 3.1 from [39] to generate V_{rd} takes nearly 3 hours and 12 minutes. The results of the greedy algorithm are displayed in Fig. 15. Compared to Test 2 for this example, Test 3 requires only 17 iterations to converge. It results in a ROM of dimension $r = 34$.

5.3.3 Test 4. Proposed error estimator

Using Algorithm 1 for the Antipodal Vivaldi antenna results in a ROM of dimension $r = 36$, with the convergence achieved in 18 iterations. The convergence of the maximum error and the corresponding effectivity are shown in Fig. 16. Although in comparison to the randomized error estimator in Test 3, the proposed approach takes one extra iteration to converge, the overall time for Test 4 is only 1 hour and 20 minutes. Moreover, the effectivity is nearly 1 for most of the iterations. The randomized estimator tending to underestimate the true error also explains why it takes fewer iterations to converge: the algorithm stops according to the already small error estimate, even before the true error is below the tolerance over the whole frequency domain.

5.4 Example IV : Dielectric Resonator Antenna

The last example we consider is the model of a dielectric resonator antenna [13] shown in Fig. 17. Reducing
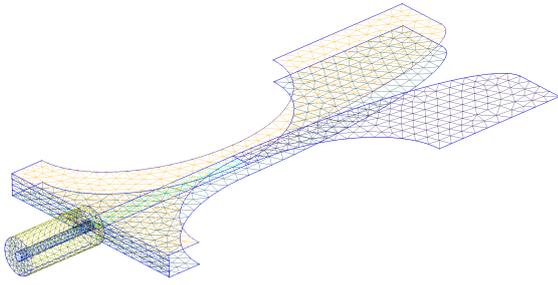
Figure 12: Antipodal Vivaldi antenna detailed in [29].

Figure 15: Antipodal Vivaldi antenna: results for Test 3.
(a) Convergence of the greedy algorithm. (b)
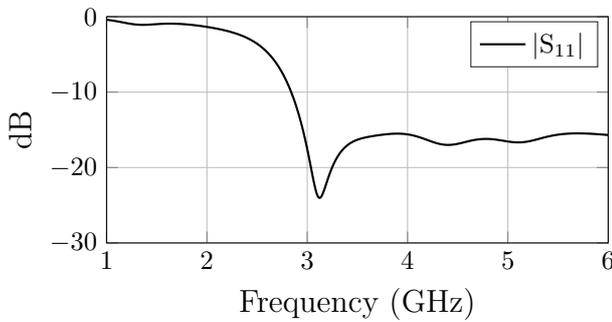Effectivity (eff).

Figure 13: Input reflection coefficient of the optimized
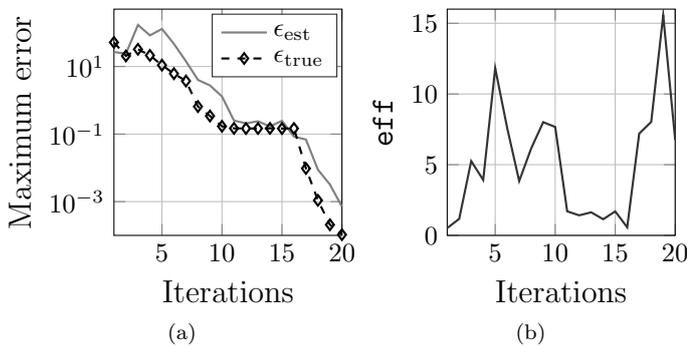Antipodal Vivaldi antenna.

Figure 14: Antipodal Vivaldi antenna: results for Test 2.
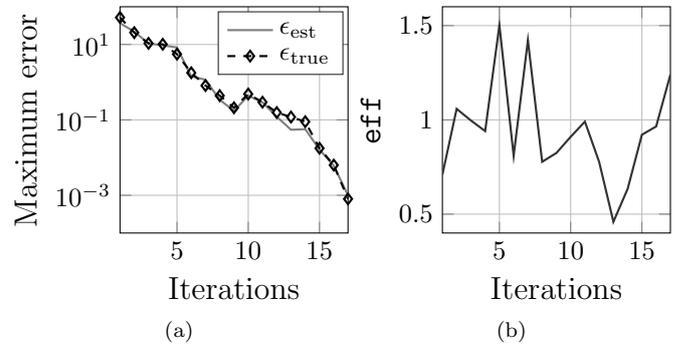(a) Convergence of the greedy algorithm. (b)
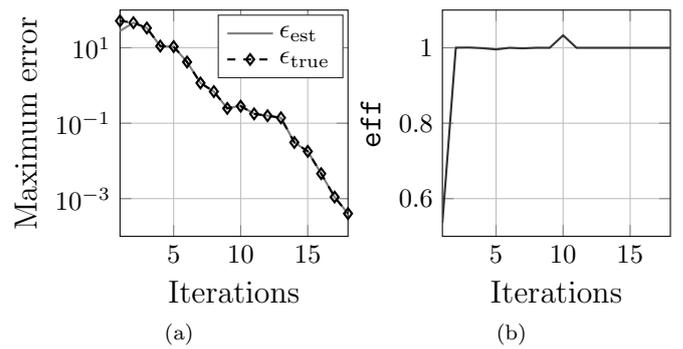Effectivity (eff).

Figure 16: Antipodal Vivaldi antenna: results for Test 4.
(a) Convergence of Algorithm 1. (b) Effectivity (eff).

the metallization part, such antennas tend to have low losses and are light weight [28]. The input reflection coefficient response is shown in Fig. 18. Among the four examples considered, this model has the largest dimension with $n = 484,294$. The frequency band of interest spans $[2.5, 4.5]$ GHz. For the training set, we sample 41 points uniformly. The tolerance for the greedy algorithms is $\mathtt{tol} = 10^{-3}$.

5.4.1 Test 2. Residual norm as a heuristic error estimator

The residual error estimator serves as a fairly good surrogate for the true error, as can be seen in Fig. 19. The algorithm converges in 12 iterations to a ROM of size $r = 24$.

5.4.2 Test 3. Randomized error estimator

We set $K = 5$, $\mathtt{tol}_{rd} = 1$ to determine V_{rd}. Once again, the random number generator $\mathtt{MersenneTwister}$ was used with the seed set to 1 to draw the random vectors. As for the previous example, this process takes up a large time, requiring almost 2 hours and 44 minutes. Fig. 20a shows the convergence of the greedy algorithm while Fig. 20b displays the effectivity of the estimator. Evidently, the randomized error estimator shows a mean effectivity around one, but with a tendency to slightly underestimate the true error. The resulting ROM of size $r = 22$ is achieved in 11 iterations.

5.4.3 Test 4. Proposed error estimator

For the final test, we apply Algorithm 1 to reduce the model of the dielectric resonator antenna. Fig. 21 shows the procedure results in a ROM with size $r = 22$, as in Test 3. However, unlike the randomized error estimator, there is no underestimation of the true error. In fact, the effectivity is almost unity, for most of the 11 iterations. Also, the time required for Algorithm 1 is about 1 hour and 49 minutes.

The time taken (in hours) for the greedy algorithms for all the four examples are summarized in Table 1. The second column gives the split for Test 1 times as: (Time for precomputing *inf-sup* constant + Time for generating V). Further, the third column of the table gives the split for the Test 3 times as: (Time for precomputing V_{rd} + Time for generating V). The greedy algorithm based on the residual norm requires the least computational time among the four error estimators. However, as illustrated in our numerical examples, its accuracy is not uniformly good. The proposed error estimator, while acceptably more expensive than the residual estimator,

Table 1: Offline time to generate projection matrix V.

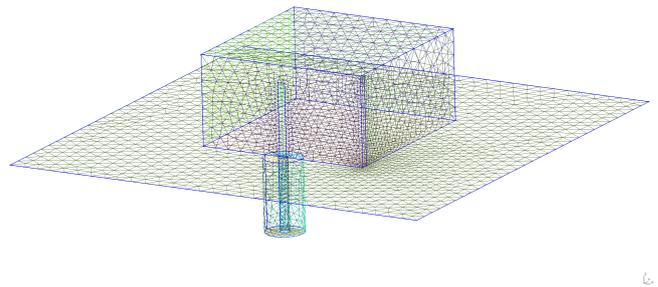| Example	Time Taken (h)			
	Test 1	Test 2	Test 3	Test 4
Dual-mode filter	$0.14 + 0.01$ $= 0.15$	0.01	$1.02 + 0.01$ $= 1.03$	0.03
SIW antenna	-	0.26	$1.32 + 0.24$ $= 1.56$	0.83
AV antenna	-	0.66	$3.20 + 0.57$ $= 3.77$	1.33
DR antenna	-	1.04	$2.73 + 0.93$ $= 3.66$	1.81

Figure 17: Dielectric resonator antenna designed in [28].

gives a far superior estimation of the true error. Also, in our tests, it requires significantly smaller offline time when compared to the randomized error estimator.

6 Conclusions

We have introduced a novel *a posteriori* error estimator capable of accurately estimating the state error, even for systems where the *inf-sup* constant is very small. Many engineering systems involving resonant electromagnetic devices, such as microwave filters, antennas show this behaviour. A waveguide filter model and models of three types of antenna are used to demonstrate the robustness of the proposed error estimator. The proposed error esti-
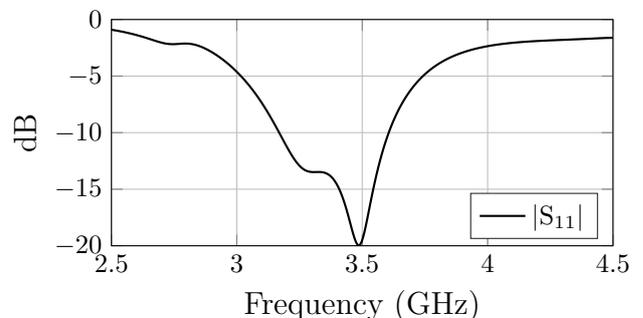

Figure 18: Reflection coefficient at the coaxial port for the dielectric resonator antenna.
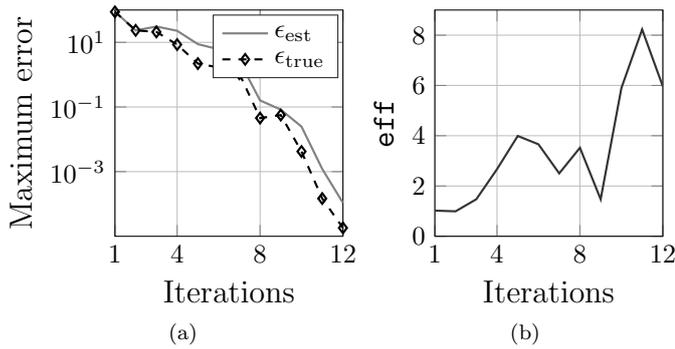
Figure 19: Dielectric resonator antenna: results for Test 2. (a) Convergence of the greedy algorithm. (b) Effectivity (`eff`).
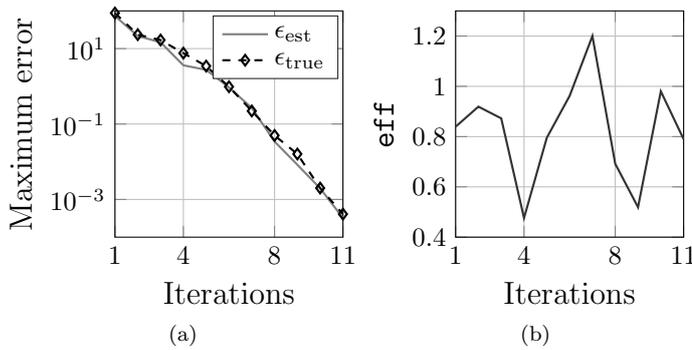

Figure 20: Dielectric resonator antenna: results for Test 3. (a) Convergence of the greedy algorithm. (b) Effectivity (`eff`).
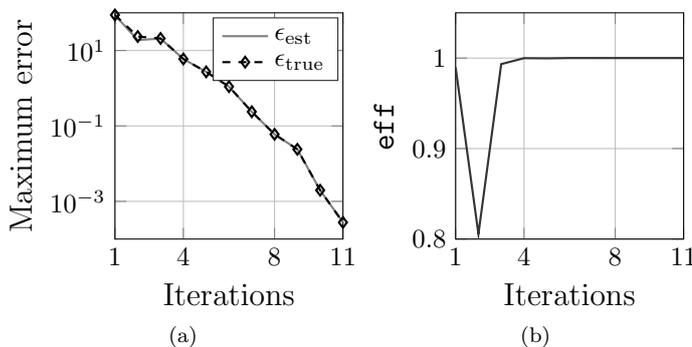

Figure 21: Dielectric resonator antenna: results for Test 4. (a) Convergence of Algorithm 1. (b) Effectivity (`eff`).

mator outperforms the standard estimator and a recently proposed one in the literature, both theoretically and numerically, thus showing its great potential in electromagnetic simulation and analysis. As a result, compact reduced order models for challenging real-life applications have been obtained.

Acknowledgments

References

[1] L. Balewski, G. Fotyga, M. Mrozowski, M. Mul, P. Sypek, D. Szypulski, and A. Lamecki. Step on it! Bringing fullwave finite-element microwave filter design up to speed. *IEEE Microwave Magazine*, 21(3):34–49, 2020. doi:10.1109/MMM.2019.2958165.

[2] R. Baltes, A. Schultschik, O. Farle, and R. Dyczij-Edlinger. A finite-element-based fast frequency sweep framework including excitation by frequency-dependent waveguide mode patterns. *IEEE Trans. Microwave Theory Tech.*, 65(7):2249–2260, 2017. doi:10.1109/TMTT.2017.2679181.

[3] Peter Benner and Lihong Feng. A robust algorithm for parametric model order reduction based on implicit moment matching. In Alfio Quarteroni and Gianluigi Rozza, editors, *Reduced Order Methods for Modeling and Computational Reduction*, chapter 6, pages 159–185. Springer, 2014. doi:10.1007/978-3-319-02090-7_6.

[4] Peter Benner, Serkan Gugercin, and Karen Willcox. A survey of projection-based model reduction methods for parametric dynamical systems. *SIAM review*, 57(4):483–531, 2015. doi:10.1137/130932715.

[5] S. Chellappa, L. Feng, and P. Benner. An adaptive sampling approach for the reduced basis method. In *Realization and Model Reduction of Dynamical Systems - A Festschrift in Honor of the 70th Birthday of Thanos Antoulas*. Springer, 2021. accepted March 2020. URL: https://arxiv.org/abs/1910.00298.

[6] Yanlai Chen, Jan S. Hesthaven, and Yvon Maday. A seamless reduced basis element method for 2D Maxwell's problem: an introduction. In *Spectral and high order methods for partial differential equations*, volume 76 of *Lect. Notes Comput. Sci. Eng.*, pages 141–152. Springer, Heidelberg, 2011. doi:10.1007/978-3-642-15337-2_11.

[7] Lorenzo Codecasa, Gian Guido Gentili, and Marco Politi. Exploiting port responses for wideband analysis of multimode lossless devices. *IEEE Trans. Microwave Theory Tech.*, 68(2):555–563, 2020. doi:10.1109/TMTT.2019.2952853.

[8] Qi I. Dai, Y. H. Lo, W. C. Chew, Y. G. Liu, and L. J. Jiang. Generalized modal expansion and reduced modal representation of 3-D electromagnetic fields. *IEEE Trans. Antennas Propagat.*, 62(2):783–793, 2014. doi:10.1109/TAP.2013.2292083.

[9] Xunwang Dang, Maokun Li, Fan Yang, and Shenheng Xu. Quasi-periodic array modeling using reduced basis from elemental array. *IEEE Journal on Multiscale and Multiphysics Computational Techniques*, 2:202–208, 2017. doi:10.1109/JMMCT.2017.2780623.

[10] Valentín de la Rubia. Reliable reduced-order model for fast frequency sweep in microwave circuits. *Electromagnetics*, 34(3-4):161–170, 2014. doi:10.1080/02726343.2014.877735.

[11] Valentín de la Rubia and Michal Mrozowski. A compact basis for reliable fast frequency sweep via the reduced-basis method. *IEEE Trans. Microwave Theory Tech.*, 66(10):4367–4382, 2018. doi:10.1109/TMTT.2018.2865957.

[12] Valentín de la Rubia, Ulrich Razafison, and Yvon Maday. Reliable fast frequency sweep for microwave devices via the reduced-basis method. *IEEE Trans. Microwave Theory Tech.*, 57(12):2923–2937, 2009. doi:10.1109/TMTT.2009.2034208.

[13] Valentín de la Rubia and Juan Zapata. MAM-a multipurpose admittance matrix for antenna design via the finite element method. *IEEE Trans. Antennas Propagat.*, 55(8):2276–2286, 2007. doi:10.1109/TAP.2007.901955.

[14] Valentín de la Rubia and Juan Zapata. Microwave circuit design by means of direct decomposition in the finite-element method. *IEEE Trans. Microwave Theory Tech.*, 55(7):1520–1530, 2007. doi:10.1109/TMTT.2007.900307.

[15] Yuandan Dong and Tatsuo Itoh. Miniaturized substrate integrated waveguide slot antennas based on negative order resonance. *IEEE Trans. Antennas Propagat.*, 58(12):3856–3864, 2010. doi:10.1109/TAP.2010.2078449.

[16] Jens L. Eftang, Anthony T. Patera, and Einar M. Rønquist. An "hp" certified reduced basis method for parametrized elliptic partial differential equations. *SIAM J. Sci. Comput.*, 32(6):3170–3200, 2010. doi:10.1137/090780122.

[17] Lihong Feng and Peter Benner. A new error estimator for reduced-order modeling of linear parametric systems. *IEEE Trans. Microwave Theory Tech.*, 67(12):4848–4859, 2019. doi:10.1109/TMTT.2019.2948858.

[18] Grzegorz Fotyga, Martyna Czarniewska, Adam Lamecki, and Michał Mrozowski. Reliable greedy multipoint model-order reduction techniques for finite-element analysis. *IEEE Antennas Wireless Propagat. Lett.*, 17(5):821–824, 2018. doi:10.1109/LAWP.2018.2817391.

[19] Sara García, Valentín de la Rubia, and Michal Mrozowski. Reduced basis approximations in microwave filters and diplexers: Inf-sup constant behavior. In *2017 IEEE MTT-S International Conference on Numerical Electromagnetic and Multiphysics Modeling and Optimization for RF, Microwave, and Terahertz Applications (NEMO)*, pages 275–277. IEEE, 2017. doi:10.1109/NEMO.2017.7964258.

[20] Christophe Geuzaine and Jean-François Remacle. Gmsh: A 3-D finite element mesh generator with built-in pre-and post-processing facilities. *Int. J. Numer. Methods Eng.*, 79(11):1309–1331, 2009. doi:10.1002/nme.2579.

[21] Martin W Hess and Peter Benner. Fast evaluation of time–harmonic maxwell's equations using the reduced basis method. *IEEE Trans. Microwave Theory Tech.*, 61(6):2265–2274, 2013. doi:10.1109/TMTT.2013.2258167.

[22] Martin W Hess, Sara Grundel, and Peter Benner. Estimating the inf-sup constant in reduced basis methods for time-harmonic Maxwell's equations. *IEEE Trans. Microwave Theory Tech.*, 63(11):3549–3557, 2015. doi:10.1109/TMTT.2015.2473157.

[23] Jan S. Hesthaven and Shun Zhang. On the use of ANOVA expansions in reduced basis methods for parametric partial differential equations. *J. Sci. Comput.*, 69(1):292–313, 2016. doi:10.1007/s10915-016-0194-9.

[24] Amit Hochman, Jorge Fernández Villena, Athanasios G Polimeridis, Luís Miguel Silveira, Jacob K White, and Luca Daniel. Reduced-order models for electromagnetic scattering problems. *IEEE Trans. Antennas Propagat.*, 62(6):3150–3162, 2014. doi:10.1109/TAP.2014.2314734.

[25] P Ingelstrom. A new set of h (curl)-conforming hierarchical basis functions for tetrahedral meshes. *IEEE Trans. Microwave Theory Tech.*, 54(1):106–114, 2006. doi:10.1109/TMTT.2005.860295.

[26] Jiahua Jiang, Yanlai Chen, and Akil Narayan. Offline-enhanced reduced basis method through adaptive construction of the surrogate training set. *J. Sci. Comput.*, 73(2-3):853–875, 2017. `doi:10.1007/s10915-017-0551-3`.

[27] Yves Konkel, Ortwin Farle, Alexander Sommer, Stefan Burgard, and Romanus Dyczij-Edlinger. A posteriori error bounds for Krylov-based fast frequency sweeps of finite-element systems. *IEEE Trans. Magn.*, 50(2):441–444, 2014. `doi:10.1109/TMAG.2013.2285442`.

[28] Bin Li and Kwok Wa Leung. Strip-fed rectangular dielectric resonator antennas with/without a parasitic patch. *IEEE Trans. Antennas Propagat.*, 53(7):2200–2207, 2005. `doi:10.1109/TAP.2005.850745`.

[29] Zheng Lou and Jian-Ming Jin. Modeling and simulation of broad-band antennas using the time-domain finite element method. *IEEE Trans. Antennas Propagat.*, 53(12):4099–4110, 2005. `doi:10.1109/TAP.2005.859905`.

[30] Alberto Monje-Real and Valentín de la Rubia. Electric field integral equation fast frequency sweep for scattering of non-penetrable objects via the reduced-basis method. *IEEE Trans. Antennas Propagat.*, 68(8):6232–6244, 2020. `doi:10.1109/TAP.2020.2992882`.

[31] Jean-Claude Nédélec. Mixed finite elements in R^3. *Numer. Math.*, 35(3):315–341, 1980. `doi:10.1007/BF01396415`.

[32] Julio L Nicolini, Dong-Yeop Na, and Fernando L Teixeira. Model order reduction of electromagnetic particle-in-cell kinetic plasma simulations via proper orthogonal decomposition. *IEEE Transactions on Plasma Science*, 47(12):5239–5250, 2019. `doi:10.1109/TPS.2019.2950377`.

[33] Anthony T Patera and Gianluigi Rozza. *Reduced basis approximation and a posteriori error estimation for parametrized partial differential equations*. MIT, 2007. MIT Pappalardo Graduate Monographs in Mechanical Engineering.

[34] Davide Pradovera. Interpolatory rational model order reduction of parametric problems lacking uniform inf-sup stability. *SIAM J. Numer. Anal.*, 58(4):2265–2293, 2020. `doi:10.1137/19M1269695`.

[35] Michał Rewieński, Adam Lamecki, and Michał Mrozowski. A goal-oriented error estimator for reduced basis method modeling of microwave devices. *IEEE Microwave Wireless Compon. Lett.*, 25(4):208–210, 2015. `doi:10.1109/LMWC.2015.2400937`.

[36] Michal Rewieński, Adam Lamecki, and Michal Mrozowski. Greedy multipoint model-order reduction technique for fast computation of scattering parameters of electromagnetic systems. *IEEE Trans. Microwave Theory Tech.*, 64(6):1681–1693, 2016. `doi:10.1109/TMTT.2016.2560167`.

[37] Gianluigi Rozza and Karen Veroy. On the stability of the reduced basis method for Stokes equations in parametrized domains. *Comput. Methods Appl. Mech. Engrg.*, 196(7):1244–1260, 2007. `doi:10.1016/j.cma.2006.09.005`.

[38] Andreas Schmidt, Dominik Wittwar, and Bernard Haasdonk. Rigorous and effective a-posteriori error bounds for nonlinear problems - application to RB methods. *Adv. Comput. Math.*, 46(2):1–30, 2020. `doi:10.1007/s10444-020-09741-x`.

[39] Kathrin Smetana, Olivier Zahm, and Anthony T Patera. Randomized residual-based error estimators for parametrized equations. *SIAM J. Sci. Comput.*, 41(2):A900–A926, 2019. `doi:10.1137/18M120364X`.

[40] A. Sommer, O. Farle, and R. Dyczij-Edlinger. Certified dual-corrected radiation patterns of phased antenna arrays by offline–online order reduction of finite-element models. *J. Comput. Phys.*, 299:22–44, 2015. `doi:10.1016/j.jcp.2015.06.024`.

[41] A. Sommer, O. Farle, and R. Dyczij-Edlinger. A new method for accurate and efficient residual computation in adaptive model-order reduction. *IEEE Trans. Magn.*, 51(3):1–4, 2015. `doi:10.1109/TMAG.2014.2352812`.

[42] W. Wang, G. N. Paraschos, and M. N. Vouvakis. Fast frequency sweep of FEM models via the balanced truncation proper orthogonal decomposition. *IEEE Trans. Antennas Propagat.*, 59(11):4142–4154, 2011. `doi:10.1109/TAP.2011.2164184`.

[43] Lifeng Wu, Yanwen Zhao, Qiangming Cai, Runren Zhang, Li Gu, Zhipeng Zhang, and Zaiping Nie. MLACE-MLFMA combined with reduced basis method for efficient wideband electromagnetic scattering from metallic targets. *IEEE Trans. Antennas Propagat.*, 67(7):4738–4747, 2019. `doi:10.1109/TAP.2019.2911352`.

[44] Li Xue and Dan Jiao. Rapid modeling and simulation of integrated circuit layout in both frequency and time domains from the perspective of inverse. *IEEE Trans. Microwave Theory Tech.*, 68(4):1270–1283, 2020. `doi:10.1109/TMTT.2020.2966699`.